STUDY OF AN ACCEPTOR IMPURITY LOCATED AT THE CENTER OF A SPHERICAL NANOHETEROSTRUCTURE

V.I. BOICHUK, I.V. BILYNSKYI, R.YA. LESHKO, I.O. SHAKLEINA

Ivan Franko Drohobych State Pedagogical University
(3, Stryiska Str., Drohobych 82100, Ukraine; e-mail: leshkoroman@mail.ru)

PACS 71.55.-i; 73.21.La; 79.60.Jv

Using the spherical 4×4 Hamiltonian, the discrete states of a hydrogenic acceptor impurity in a spherical GaSb/AlSb nanoheterostructure with various quantum-dot sizes are determined. The energies obtained are compared with those calculated without consideration of the complex structure of the valence band. The calculations are carried out for both finite and infinite potentials at the heterostructure interface. The selection rules are found for intraband optical transitions between hole levels. The average distances and the transition probabilities for holes are determined as functions of the quantum-dot sizes.

1. Introduction

Recently, low-dimensional heterostructures have become a subject of both theoretical and experimental researches in solid-state physics. A considerable attention is given to studying quantum dots (QDs). Since the charge carriers possess a completely discrete spectrum in them, QDs have improved optical properties, and they are researched to be applied in diode lasers, amplifiers, and biological sensors.

Many works are devoted to the study of properties of electrons in QDs. Since the conduction band in the majority of crystals under consideration can be described by a parabolic dispersion law, effective masses were introduced, and a simple Schrödinger equation was derived. The use of such an approximation and the application of the model of dielectric continuum in theoretical works provide good agreement with experimental data. On the basis of these principles, exact solutions of the Schrödinger equation were found for QDs with symmetric shapes, the calculations of electron discrete states were carried out, and the probabilities of interlevel transitions were found [1, 2]. The influence of polarization charges [3, 4] and deformation [5, 6] at the heterostructure interfaces on the electron energy spectrum was studied, and the structure of energy subbands in QD arrays was determined [7]. Impurities in QDs can considerably change the localized states and, consequently, the QD properties. In works [8–12], the first theoretical researches of impurity donor states in spherical QDs were carried out, and the exact solutions of the Schrödinger equation with the Coulomb potential interaction between particles were obtained. In work [13], it was shown that taking the exact solution of the Poisson and Schrödinger equations for a hydrogenic donor impurity into account somewhat changes the electron spectrum in comparison with the results of works [8–12].

The valence band of many semiconductors is degenerate. Work [14] is one of the first works, where general spherically symmetric solutions for even and odd hole states with the total angular momentum f were obtained in the framework of the multiband crystal model. The shallow acceptors in massive semiconductors were studied in work [15], where, on the basis of works [14, 16, 17], the hole Hamiltonian in the spherical approximation was derived, and calculations for acceptors were carried out in the cases of strong and weak spin-orbit interaction. The hole quantization and the absorption edge in spherical microcrystals of semiconductors with a complicated band structure were described in work [18]. In work [19], the solutions of the Schrödinger equation for QDs were obtained in the framework of the spherical approximation, and the probability of optical transitions was analyzed in the cases of finite and infinite band discontinuities at the heterostructure interfaces. Again, in work

[20], in the framework of the four-band model, the exciton states in spherical QDs and the influence of an electric field on them were studied, the Stark effect was analyzed, and the influence of an electric field on the matrix elements of the dipole moment was described, the analysis being carried out in the framework of the model of infinite band discontinuity at the heterostructure interfaces. On the other hand, in work [21], the 8×8 Hamiltonian was obtained, the boundary conditions were formulated, and the quasiparticle spectra were calculated numerically for the model of finite band discontinuity.

The presence of donor and acceptor impurities in QDs can considerably change localized states. Though the calculations for acceptor states were carried out in various works – e.g. in works [15, 22] for massive crystals and in work [23] for thin films – the acceptor states and their influence on QD properties still remain insufficiently studied up to now. Therefore, the aim of this work was to analyze the influence of dimensions of a spherical QD, with an acceptor impurity and without it, on the hole energy spectrum, taking a complicated structure of the valence band into account. Here, we will also calculate the average distances for the hole, find the selection rules for optical transitions between the hole levels resulted from the size quantization, and determine the probabilities of such transitions. Specific calculations were carried out for a spherical GaSb/AlSb nanoheterosystem.

2. Statement of the Problem and Its Solution

2.1. 4×4 *Hamiltonian*

Let us consider a nanoheterosystem GaSb/AlSb with a spherical QD of radius a which contains an acceptor impurity at the center. We suppose that the valence band in this heterostructure is four-time degenerate at the point $k = 0$, because it is formed by crystals with a wide energy gap and the strong spin-orbit interaction, so that the conduction and spin-split bands can be neglected. Therefore, certain difficulties arise at the solution of the Schrödinger equation. However, the problem can be simplified, if one neglects the corrugation of isoenergetic surfaces in the k-space (the spherical approximation).

Let the energy axis in the valence band be directed "downward". Then, the spherical Hamiltonian – in the effective mass approximation, without taking the conduction and spin-split bands into account, and assuming that the hole can be assigned the spin $j = 3/2$ – looks like

$$\mathbf{H} = \frac{1}{2}\left(\gamma_1 + \frac{5}{2}\gamma\right)\mathbf{p}^2 - \gamma\left(\mathbf{pJ}\right)^2 + \Pi\left(r\right), \tag{1}$$

where

$$\Pi\left(r\right) = V\left(r\right) + U\left(r\right) \tag{2}$$

is the potential energy; $\gamma = 1/5\left(3\gamma_3 + 2\gamma_2\right)$; γ_1, γ_2, and γ_3 are the Luttinger parameters which are designated as follows for different heterostructure regions:

$$\left(\gamma_1 \;\; \gamma_2 \;\; \gamma_3\right) = \begin{cases} \left(\gamma_1^{\text{in}} \;\; \gamma_2^{\text{in}} \;\; \gamma_3^{\text{in}}\right), & r \le a, \\ \left(\gamma_1^{\text{out}} \;\; \gamma_2^{\text{out}} \;\; \gamma_3^{\text{out}}\right), & r > a, \end{cases}$$

and $\mathbf{J} = \mathbf{i}J_x + \mathbf{j}J_y + \mathbf{k}J_z$ is the operator of spin moment $3/2$. On the basis of the Poisson equation solution, the energy of interaction between an acceptor ion and a hole is given by the formula

$$V\left(r\right) = \begin{cases} -\dfrac{1}{\varepsilon^{\text{in}} r} - \dfrac{\varepsilon^{\text{in}} - \varepsilon^{\text{out}}}{\varepsilon^{\text{in}}\varepsilon^{\text{out}} a}, & r \le a, \\ -\dfrac{1}{\varepsilon^{\text{out}} r}, & r > a, \end{cases} \tag{3}$$

and the potential energy associated with a band discontinuity (the confinement potential) is selected in the form of a spherical rectangular potential well:

$$U\left(r\right) = \begin{cases} 0, & r \le a, \\ U_0, & r > a. \end{cases} \tag{4}$$

In all formulas, we use the system of units with $m_0 = 1$, $\hbar = 1$, and $e = 1$. The spherically symmetric Hamiltonian (1) commutes with the operator of total angular momentum $\mathbf{F} = \mathbf{L} + \mathbf{J}$, in which the orbital moment $\mathbf{L}$ characterizes the "macroscopic" orbital motion which is described by the effective mass method.

The wave function that describes a hole in the presence of an acceptor can be expressed as a four-component column function, and the even and odd states can be separated [14, 18]:

$$\begin{cases} \psi^I = R^I_{a,2}\left(r\right)\Phi^{(4)}_{f-3/2}\left(\theta,\varphi\right) + R^I_{a,1}\left(r\right)\Phi^{(4)}_{f+1/2}\left(\theta,\varphi\right), \\ \psi^{II} = R^{II}_{a,2}\left(r\right)\Phi^{(4)}_{f-1/2}\left(\theta,\varphi\right) + R^{II}_{a,1}\left(r\right)\Phi^{(4)}_{f+3/2}\left(\theta,\varphi\right). \end{cases} \tag{5}$$

The functions $\Phi^{(4)}$ are four-component spinors that correspond to the spin $j = 3/2$. In the spinors, the quantum numbers f and l are connected as follows:

$$\Phi^{(4)}_{f-3/2}\left(\theta,\varphi\right), \;\; f = l + \tfrac{3}{2}; \qquad \Phi^{(4)}_{f+1/2}\left(\theta,\varphi\right), \;\; f = l - \tfrac{1}{2};$$
$$\Phi^{(4)}_{f-1/2}\left(\theta,\varphi\right), \;\; f = l + \tfrac{1}{2}; \qquad \Phi^{(4)}_{f+3/2}\left(\theta,\varphi\right), \;\; f = l - \tfrac{3}{2}.$$

Depending on the f- and l-values, the functions ψ^I and ψ^{II} are even or odd. Substituting functions (5) into the Schrödinger equation with Hamiltonian (1), multiplying by the corresponding conjugate spinors, and integrating over the angular variables, we obtain two systems of coupled differential equations of the second order for the even and odd states. These two systems are written down in the form of a matrix equation

$$\frac{\gamma_1}{2}\left(\begin{array}{cc} -(1+C_1)\,\mathbf{\Delta}_l & C_2\mathbf{A}^-_{l+1}\mathbf{A}^-_{l+2} \\ C_2\mathbf{A}^+_{l+1}\mathbf{A}^+_l & -(1+C_3)\,\mathbf{\Delta}_{l+2}\end{array}\right)\times \\ \times\left(\begin{array}{c} R^i_{a,2} \\ R^i_{a,1}\end{array}\right)+\Pi(r)\left(\begin{array}{c} R^i_{a,2} \\ R^i_{a,1}\end{array}\right)=E_a\left(\begin{array}{c} R^i_{a,2} \\ R^i_{a,1}\end{array}\right), \tag{6}$$

where $i = I$ for even states and $i = II$ for odd ones. The coefficients in Eq. (6) are written down, by using 6-j symbols

$$C_1 = C_1(f,l) = \mu\sqrt{5}\,(-1)^{3/2+l+f}\times \\ \times\left\{\begin{array}{ccc} l & l & 2 \\ 3/2 & 3/2 & f\end{array}\right\}\sqrt{\frac{2l\,(2l+1)\,(2l+2)}{(2l+3)\,(2l-1)}},$$

$$C_2 = C_2(f,l) = \mu\sqrt{30}\,(-1)^{3/2+l+f}\times \\ \times\left\{\begin{array}{ccc} l+2 & l & 2 \\ 3/2 & 3/2 & f\end{array}\right\}\sqrt{\frac{(l+1)\,(l+2)}{2l+3}},$$

$$C_3 = -C_1,\quad (C_1)^2+(C_2)^2=\mu^2,\quad C_2/\mu>0,\quad \mu=\frac{2\gamma}{\gamma_1}.$$

The operators in Eq. (6) are defined by the relations

$$\mathbf{A}^+_l = -\frac{\partial}{\partial r}+\frac{l}{r},\quad \mathbf{A}^-_l=\frac{\partial}{\partial r}+\frac{l+1}{r},$$

$$\mathbf{\Delta}_l = \frac{\partial^2}{\partial r^2}+\frac{2}{r}\frac{\partial}{\partial r}-\frac{l\,(l+1)}{r^2}. \tag{7}$$

Equation (6) with potential (2) cannot be solved exactly. Therefore, the approximate methods of quantum mechanics are used.

2.2. Discrete spectrum of a hole in a QD without impurity

Let us find the solution of the Schrödinger equation for a QD charge without impurity. In this case,

$$\Pi(r)=U(r),\quad E_a=E^i,\quad \left(\begin{array}{c} R^i_{a,2}(r) \\ R^i_{a,1}(r)\end{array}\right)=\left(\begin{array}{c} R^i_2(r) \\ R^i_1(r)\end{array}\right).$$

Then, Eq. (6) allows exact solutions which can be expressed in terms of of Bessel functions of the first kind and modified Bessel functions of the second kind. The solutions can be found for both coordinate regions:
1) at $r \le a$,

$$R^{i,\mathrm{in}}_2(r) = B_1\frac{C^{\mathrm{in}}_1-\mu^{\mathrm{in}}}{\sqrt{(\mu^{\mathrm{in}})^2-\left(C^{\mathrm{in}}_1\right)^2}}\frac{\mathrm{J}_{l+\frac12}\left(\frac{k^ir}{\sqrt{1-(\mu^{\mathrm{in}})^2}}\right)}{\sqrt{r}}+ \\ +B_2\frac{C^{\mathrm{in}}_1+\mu^{\mathrm{in}}}{\sqrt{(\mu^{\mathrm{in}})^2-\left(C^{\mathrm{in}}_1\right)^2}}\frac{\mathrm{J}_{l+\frac12}\left(\frac{k^ir}{\sqrt{1+(\mu^{\mathrm{in}})^2}}\right)}{\sqrt{r}}, \tag{8}$$

$$R^{i,\mathrm{in}}_1(r) = B_1\frac{J_{l+\frac52}\left(\frac{k^ir}{\sqrt{1-(\mu^{\mathrm{in}})^2}}\right)}{\sqrt{r}}+ \\ +B_2\frac{J_{l+\frac52}\left(\frac{k^ir}{\sqrt{1+(\mu^{\mathrm{in}})^2}}\right)}{\sqrt{r}}, \tag{9}$$

where $k^i=\sqrt{\frac{2}{\gamma^{\mathrm{in}}_1}E^i}$;
2) at $r > a$,

$$R^{i,\mathrm{out}}_2(r) = D_1\frac{-C^{\mathrm{out}}_1+\mu^{\mathrm{out}}}{\sqrt{(\mu^{\mathrm{out}})^2-(C^{\mathrm{out}}_1)^2}}\frac{K_{l+\frac12}\left(\frac{\lambda^ir}{\sqrt{1-(\mu^{\mathrm{out}})^2}}\right)}{\sqrt{r}}+ \\ +D_2\frac{-C^{\mathrm{out}}_1-\mu^{\mathrm{out}}}{\sqrt{(\mu^{\mathrm{out}})^2-(C^{\mathrm{out}}_1)^2}}\frac{K_{l+\frac12}\left(\frac{\lambda^ir}{\sqrt{1+(\mu^{\mathrm{out}})^2}}\right)}{\sqrt{r}}, \tag{10}$$

$$R^{i,\mathrm{out}}_1(r) = D_1\frac{K_{l+\frac52}\left(\frac{\lambda^ir}{\sqrt{1-(\mu^{\mathrm{out}})^2}}\right)}{\sqrt{r}}+ \\ +D_2\frac{K_{l+\frac52}\left(\frac{\lambda^ir}{\sqrt{1+(\mu^{\mathrm{out}})^2}}\right)}{\sqrt{r}}, \tag{11}$$

where $\lambda^i=\sqrt{\frac{2}{\gamma^{\mathrm{out}}_1}(U_0-E^i)}$.

Knowing the exact solutions, it is possible to use the boundary conditions to determine the hole energy and the average distance

$$\langle r\rangle = \int dr r^2\left(\left|R^i_2(r)\right|^2+\left|R^i_1(r)\right|^2\right)r. \tag{12}$$

2.3. Boundary conditions

In order to obtain the boundary conditions for a spherical QD, two conditions were used: the continuity of the radial wave function and the normal component of the probability density flux vector through the QD spherical surface. The continuity of the wave functions at the heterostructure interface gives two equations which are written down in the form of a column matrix:

$$\left(\begin{array}{c} R_2^{i,\mathrm{in}}(r) \\ R_1^{i,\mathrm{in}}(r) \end{array} \right)\Bigg|_{r=a} = \left(\begin{array}{c} R_2^{i,\mathrm{out}}(r) \\ R_1^{i,\mathrm{out}}(r) \end{array} \right)\Bigg|_{r=a}. \tag{13}$$

To determine the normal component of the probability density flux vector, we calculated the normal component of the velocity operator vector $\mathbf{V}_r = \mathbf{r}/r\,(\partial\mathbf{H}/\partial\mathbf{p})$ which is proportional to the normal component of the probability density flux vector. Then, the operator is written down in the spinor representation for even and odd states. Using the explicit form of operators, two more conditions used for matching the wave function are obtained:

a) for even states,

$$\begin{array}{l} \left(\begin{array}{cc} \mathbf{T}_{11}^{I,\mathrm{in}} & \mathbf{T}_{12}^{I,\mathrm{in}} \\ \mathbf{T}_{21}^{I,\mathrm{in}} & \mathbf{T}_{22}^{I,\mathrm{in}} \end{array} \right) \left(\begin{array}{c} R_2^{I,\mathrm{in}}(r) \\ R_1^{I,\mathrm{in}}(r) \end{array} \right)\Bigg|_{r=a} = \\ = \left(\begin{array}{cc} \mathbf{T}_{11}^{I,\mathrm{out}} & \mathbf{T}_{12}^{I,\mathrm{out}} \\ \mathbf{T}_{21}^{I,\mathrm{out}} & \mathbf{T}_{22}^{I,\mathrm{out}} \end{array} \right) \left(\begin{array}{c} R_2^{I,\mathrm{out}}(r) \\ R_1^{I,\mathrm{out}}(r) \end{array} \right)\Bigg|_{r=a}; \end{array} \tag{14}$$

b) for odd ones,

$$\begin{array}{l} \left(\begin{array}{cc} \mathbf{T}_{11}^{II,\mathrm{in}} & \mathbf{T}_{12}^{II,\mathrm{in}} \\ \mathbf{T}_{21}^{II,\mathrm{in}} & \mathbf{T}_{22}^{II,\mathrm{in}} \end{array} \right) \left(\begin{array}{c} R_2^{II,\mathrm{in}}(r) \\ R_1^{II,\mathrm{in}}(r) \end{array} \right)\Bigg|_{r=a} = \\ = \left(\begin{array}{cc} \mathbf{T}_{11}^{II,\mathrm{out}} & \mathbf{T}_{12}^{II,\mathrm{out}} \\ \mathbf{T}_{21}^{II,\mathrm{out}} & \mathbf{T}_{22}^{II,\mathrm{out}} \end{array} \right) \left(\begin{array}{c} R_2^{II,\mathrm{out}}(r) \\ R_1^{II,\mathrm{out}}(r) \end{array} \right)\Bigg|_{r=a}, \end{array} \tag{15}$$

where the following notations for the operators were introduced:

$$\mathbf{T}_{11}^{I} = \frac{b_1^I}{r} + b_2^I \frac{\partial}{\partial r} - 3g_4^{f,p}\frac{\chi_1^I}{r};$$

$$\mathbf{T}_{12}^{I} = -b_3^I \mathbf{Q}_{f+1/2}^{(-1)}; \quad \mathbf{T}_{21}^{I} = b_3^I \mathbf{Q}_{f-3/2}^{(1)};$$

$$\mathbf{T}_{22}^{I} = -\frac{b_1^I}{r} + b_4^I \frac{\partial}{\partial r} + g_{-8}^{f,p}\frac{\chi_2^I}{r};$$

$$\mathbf{T}_{11}^{II} = \frac{b_1^{II}}{r} + b_2^{II} \frac{\partial}{\partial r} - 3g_4^{f,p}\frac{\chi_1^{II}}{r};$$

$$\mathbf{T}_{12}^{II} = -b_3^{II} \mathbf{Q}_{f+1/2}^{(-1)}; \quad \mathbf{T}_{21}^{II} = b_3^{II}\ \mathbf{Q}_{f-3/2}^{(1)};$$

$$\mathbf{T}_{22}^{II} = -\frac{b_1^{II}}{r} + b_4^{II} \frac{\partial}{\partial r} + g_{-8}^{f,p}\frac{\chi_2^{II}}{r};$$

$$\mathbf{Q}_l^{(m)} = -m\frac{\partial}{\partial r} + \frac{l + 1/2\,(1-m)}{r};$$

and the coefficients look like

$$b_1^I = \frac{3\,(2f-3)}{4f}\gamma, \quad b_2^I = \frac{2f-3}{2f}\gamma + \gamma_1,$$

$$b_3^I = \frac{\gamma}{2}\frac{\sqrt{3}}{f}\sqrt{4f\,(f+1)-3}, \qquad b_4^I = -\frac{2f-3}{2f}\gamma + \gamma_1,$$

$$\chi_1^I = \left(f - \frac{3}{2}\right)(1 - 5\gamma + \gamma_1),$$

$$\chi_2^I = \frac{1}{6}\,(2f+9)\,(-1 + 5\gamma - \gamma_1),$$

$$b_1^{II} = \frac{3\,(2f+5)}{4\,(f+1)}\gamma, \quad b_2^{II} = -\frac{2f+5}{2\,(f+1)}\gamma + \gamma_1,$$

$$b_3^{II} = \gamma\sqrt{3}\sqrt{1 - \frac{3}{2f+2}}\sqrt{1 + \frac{1}{2f+2}},$$

$$b_4^{II} = \frac{2f+5}{2\,(f+1)}\gamma + \gamma_1,$$

$$\chi_1^{II} = \left(f + \frac{5}{2}\right)(-1 + 5\gamma - \gamma_1),$$

$$\chi_2^I = \frac{1}{6}\,(2f-7)\,(1 - 5\gamma + \gamma_1),$$

$$g_n^{f,p} = p\,(f + 1/2 - p\,n/2),$$

and $p = \pm 1$ for even and odd states, respectively.

Hence, we determine the conditions the radial wave functions for even and odd states must satisfy. Using the boundary conditions (13), (14), or (15), we obtain a linear homogeneous system of four equations for the coefficients B_1, B_2, D_1, and D_2. By zeroing the determinant of this system, we obtain an equation for finding the hole energy.

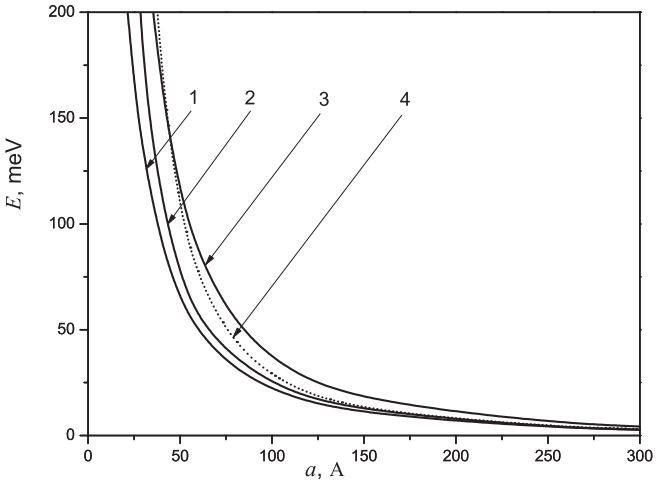

Fig. 1. Hole energies calculated in the finite potential model (solid curves): (*1*) $1S_{3/2}$, (*2*) $1P_{3/2}$, and (*3*) $1P_{5/2}$; (*4*) hole energy in the ground state $1S_{3/2}$ calculated in the infinite potential model (dotted curve)

2.4. Energy spectrum of an acceptor impurity

As was already marked above, Eq. (6) with the potential energy (2) cannot be solved exactly. Therefore, we present the wave function of an acceptor in the form of an expansion in the functions obtained for the problem without impurity:

$$\begin{pmatrix} R^i_{a,2}(r) \\ R^i_{a,1}(r) \end{pmatrix} = \sum_n a_n \begin{pmatrix} R^i_{2,n}(r) \\ R^i_{1,n}(r) \end{pmatrix}, \tag{16}$$

where n is the specific hole state. The expansion was carried out in terms of states with identical parity at the fixed quantum numbers f and l. When substituting expression (16) into the Schrödinger equation (6), it is necessary to take into account that $\begin{pmatrix} R^i_{2,n} \\ R^i_{1,n} \end{pmatrix}$ are the characteristic functions of the radial impurity-free Hamiltonian, and E^i_n is its eigenvalue. Multiplying the result by the conjugate row vector $\begin{pmatrix} R^{i*}_{2,m} & R^{i*}_{1,m} \end{pmatrix}$ and integrating over the coordinate r, we obtain a homogeneous system of equations for the coefficients a_n,

$$\sum_n \left(\left(E^i_n - E_a \right) \delta_{mn} + V_{mn} \right) a_n = 0, \tag{17}$$

where $V_{mn} = \int dr r^2 V(r) \left[\left(R^i_{2,m} \right)^* R^i_{2,n} + \left(R^i_{1,m} \right)^* R^i_{1,n} \right]$. By equating the determinant of the system to zero, we obtain an equation, from which the acceptor energy is determined.

2.5. Probabilities of interlevel transitions

In the dipole approximation, the probability of optical transitions is proportional to the squared matrix element of the dipole moment of interlevel transitions. The calculation of the angular part of integrals and the analysis of the radial part of the matrix element enabled us to establish that the following transitions between states are possible:

1) even–even, if $f' - f = \pm 1$ and $M'_f - M_f = 0$;
2) odd–odd, if $f' - f = \pm 1$ and $M'_f - M_f = 0$;
3) even–odd, if $f' - f = 0$ and $M'_f - M_f = 0$.

Here, M_f is the quantum number that corresponds to the projection of the total angular momentum. Knowing the states between which the transitions are possible, one can immediately calculate the square of the matrix element of the dipole moment of interlevel transitions:

$$|\mathbf{D}_{mn}|^2 = \left| \int d\mathbf{r} \left(\psi_m \right)^+ \mathbf{r} \psi_n \right|^2 . \tag{18}$$

Using the formulas presented above, we calculated the energy spectrum of an acceptor hole, the average distances, and the probabilities of interlevel transitions.

3. Analysis of the Results Obtained

All calculations were carried out for a GaSb/AlSb heterosystem, the crystal parameters of which were reported in works [15, 24].

In Fig. 1, the dependences of the ground – $1S_{3/2}$ ($f = 3/2$, $l = 0$) – and excited – $1P_{3/2}$ ($f = 3/2$, $l = 1$) and $1P_{5/2}$ ($f = 5/2$, $l = 1$) – state energies of the hole in a spherical QD without impurity on the QD radius are depicted. As one would expect, a reduction of the QD radius enhances the spatial restriction of the hole; therefore, its energy grows. The figure demonstrates that the ground state energy calculated in the framework of the finite-potential model lies below its counterpart calculated for the infinite potential. However, for extremely large radii, this energy difference vanishes, because the influence of heterostructure interfaces becomes infinitesimal. The figure also makes it evident that the calculated energy levels are arranged in the following order: $1S_{3/2}$, $1P_{3/2}$, and $1P_{5/2}$.

If the complicated band structure is not taken into account, only the heavy- or light-hole band is chosen for calculations, and the effective mass for, respectively, heavy, m_h, or light, m_l, holes is introduced – this was done many times and in plenty of works; see, e.g., works

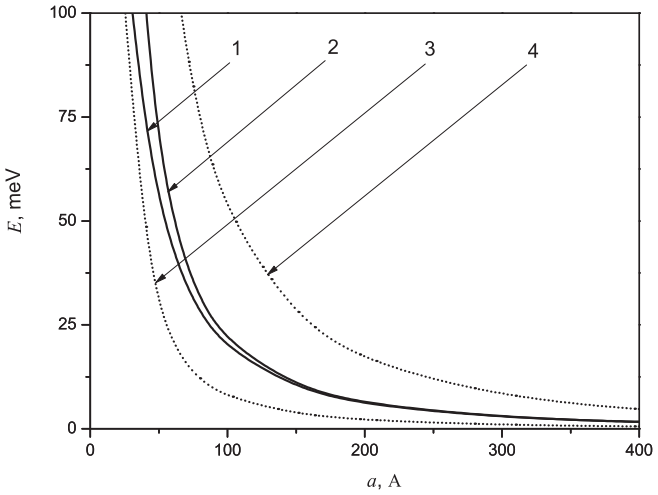

Fig. 2. Energies of the hole ground state calculated in the framework of different models

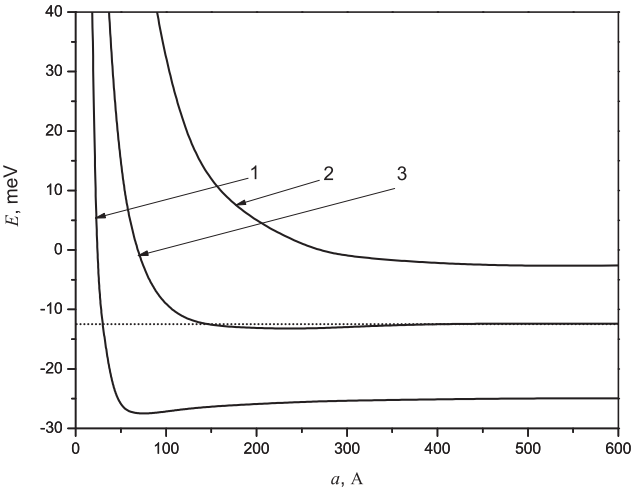

Fig. 3. Ground state energies of an acceptor impurity hole for the one-band (curves *1* and *2*) and four-band (curve *3*) models

[7, 25] – we obtain a simple equation

$$\left(-\frac{1}{2}\nabla\frac{1}{m_{\left\{ \begin{smallmatrix} h \\ l \end{smallmatrix} \right\}}}\nabla + U(r) \right) \Psi = E\Psi,$$

the solutions of which are spherical Bessel and spherical Hankel functions of the first kind.

For the sake of comparison between the results of calculations, we show the plots for the ground state energy of a hole in Fig. 2 which were calculated by considering the 4×4 Hamiltonian and the boundary conditions of work [19] (curve *1*), the 4×4 Hamiltonian and boundary conditions (13) and (14) (curve *2*), the heavy-hole band (curve *3*), and the light-hole band (curve *4*). The calculations were carried out in the case of a finite potential at the heterointerface. One can see that the energy obtained in the one-band approximation for heavy holes is lower than that calculated in the four-band model. The energy of light holes is naturally higher than the energy of heavy holes. In the case where the boundary conditions of work [19] are used (they were obtained by neglecting the non-diagonal terms in the radial Hamiltonian), the hole energies obtained for radii $a \geq 150$ Å become identical to those obtained in the case of the exact boundary conditions (curves *1* and *2* coincide). However, at small radii, the energies under the indicated boundary conditions are different, because, when the QD sizes become smaller, the heterostructure interfaces affect the energy spectrum more strongly. For small radii, the hole energy calculated in work [19] tends to the heavy-hole energy for a QD of the GaSb/AlSb heterosystem. Hence, the boundary conditions of work [19] can be used for the determination of the hole energy in a wide enough region of variation of the QD radius, $a \geq 150$ Å. In this article, however, we use the boundary conditions (13)–(15) for further calculations in the framework of the four-band model.

We also studied the dependence of the acceptor energy on the QD radius. For the specific radius a and quantum numbers f and l, expansion (16) contains the same number of terms, as the number of hole states in the impurity-free case with the same parameters a, f, and l for a finite potential at the heterointerface. The same number of terms was taken for the infinite-potential model.

If a complicated structure of the valence band is neglected, and the heavy- and light-hole bands are considered separately, we obtain the Schrödinger equation, the solutions of which for an impurity can be presented in the form of Whittaker and Coulomb functions [11–13]. In Fig. 3, we give the acceptor ground state energy which was calculated for a finite potential at the heterointerfaces and taking the heavy-hole band (curve *1*), the light-hole band (curve *2*), the 4×4 Hamiltonian, and boundary conditions (13) and (14) (curve *3*) into consideration.

Similarly to what occurs for a hole without acceptor impurity, taking the heavy-hole band into account only underestimates the acceptor state energy, and the consideration of the light-hole band overestimates it. The energy of the acceptor impurity ground state calculated within the four-band model approaches the corresponding energy in a massive crystal (horizontal dotted line) [15] for large QD radii. The consideration of the exact

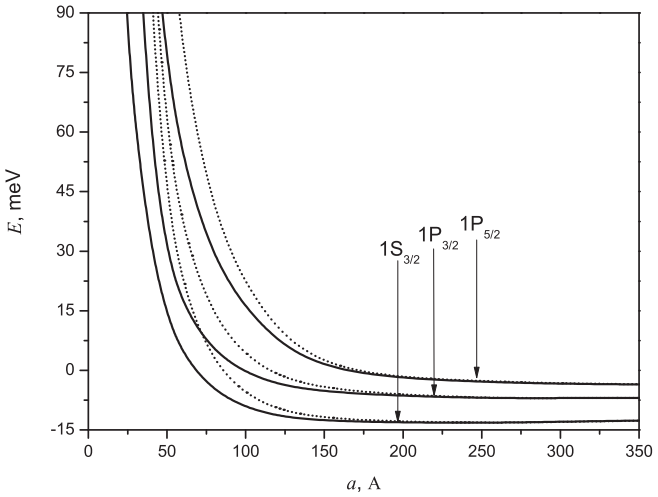

Fig. 4. Energy spectra of an acceptor impurity hole for finite (solid curves) and infinite (dotted curves) potentials at the heterointerface

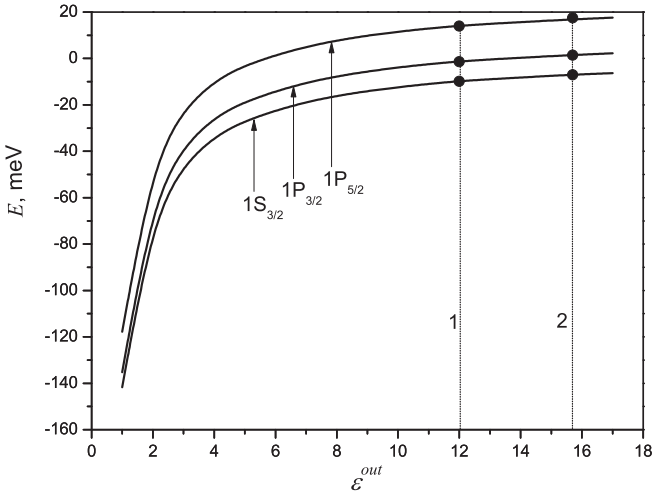

Fig. 5. Dependences of the ground and excited acceptor hole state energies on the dielectric permittivity of the matrix at the fixed QD radius $a = 100$ Å

potential energy of interaction between the hole with the impurity ion (formula (3)) gives rise to a nonmonotonous dependence of the energy on the QD radius in all three models. First, a reduction of QD dimensions is accompanied by a slight energy decrease, due to the growth of the effective potential well, whereas a subsequent reduction leads to the energy growth, because the spatial confinement of the hole prevails over the increase of the effective potential well.

In the framework of the four-band model, besides the ground hole state, we also calculated the excited states

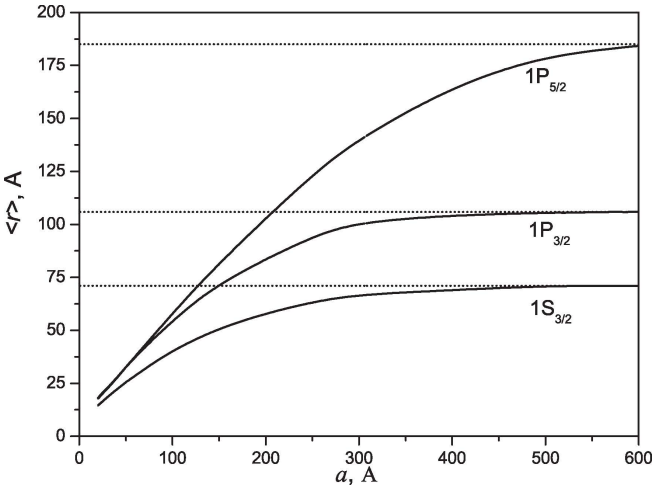

Fig. 6. Dependences of the average acceptor hole distances on the QD radius

for finite and infinite potentials at the medium interface. The results of calculations are graphically demonstrated in Fig. 4. The behavior of the excited states is similar to that of the ground one. That is, at large QD radii, the energies of states tend to the corresponding energies in a massive GaSb crystal; a size reduction leads to an insignificant smooth fall of the energy, due to an increase of the effective potential well depth followed by a drastic growth as a result of the spatial confinement prevalence over the growth of the effective potential well depth.

We also calculated the dependences of the energies of acceptor levels on the dielectric permittivity of the matrix at the constant QD radius $a = 100$ Å and a finite potential at the heterointerfaces (Fig. 5). The points of intersection with the vertical straight line *1* correspond to the dielectric permittivity of AlSb, and those with the straight line *2* do to the case where the dielectric permittivities of the QD and the matrix are identical. From the figure, one can see that a decrease of ε^{out} leads to a reduction of the acceptor impurity energy; it is associated with the growth of the parameter $\left(\varepsilon^{\text{in}} - \varepsilon^{\text{out}}\right)/(\varepsilon^{in}\varepsilon^{\text{out}}a)$, which governs the magnitude of the effective potential well.

To analyze the spatial distribution of holes, we calculated the average distances, as functions of the QD radius (Fig. 6). The figure demonstrates that, at large QD radii, the average distances of the acceptor hole tends to the corresponding values for a massive GaSb crystal. A decrease of the radius localizes the electron in the QD, so that the average distances also decrease. However, for the three states under consideration and the QD radii $a > 20$ Å, i.e. in the range where the effective mass ap-

proximation is valid, the average distances are less that the radius, which means that the hole is located in the QD with a higher probability.

When studying the physical processes which are responsible for the light absorption and emission, it is important to know the square of the matrix element of the dipole moment of hole interlevel transitions. We calculated this quantity for the transitions between the acceptor hole states $1S_{3/2}$, $1P_{3/2}$, and $1P_{5/2}$. In Table, the results of corresponding calculations are quoted. One can see that the QD radius growth increases the value of $|\mathbf{D}_{mn}|^2$ for all calculated states. In addition, the transitions $1S_{3/2} \leftrightarrow 1P_{5/2}$ turn out by an order of magnitude more probable than the transitions $1S_{3/2} \leftrightarrow 1P_{3/2}$. The level $1P_{3/2}$ is characterized by a large lifetime in comparison with other excited states. Proceeding from this fact, we suppose that, at experimental measurements of absorption and luminescence spectra, the Stokes shift is to be observed, the magnitude of which should depend on the QD radius and the dielectric permittivity of the matrix. For example, for a QD in the heterosystem GaSb/AlSb with an acceptor impurity, the Stokes shift $\Delta\lambda_{\rm st} = 78.72$ μm for the size $a = 50$ Å, and $\Delta\lambda_{\rm st} = 144.83$ μm for $a = 100$ Å. If the dielectric permittivity of the matrix is supposed to be $\varepsilon^{\rm out} = 5$, we obtain that $\Delta\lambda_{\rm st} = 80.59$ and 149.31 μm for the QD size $a = 50$ and 100 Å, respectively.

4. Conclusions

In this work, on the basis of the four-band model, a system of coupled differential equations of the second order was derived for a spherical heterostructure GaSb/AlSb and used to calculate the hole energy. A comparison of the results obtained with those calculated for the one-band model was carried out. The consideration of a complicated valence band spectrum gave rise to a lower hole energy than that of the light-hole band only, and to a higher hole energy than the consideration of the heavy-hole band only. In view of the exact hole solutions in a spherical QD and the exact solution of the Poisson equation, the potential energy of interaction between the hole and the impurity center is written down, and the approximate wave function of acceptor is constructed. The behavior of the average acceptor hole distances at the variation of the QD radius is investigated, which enabled us to reveal that the hole is located in the QD with a higher probability at all QD radii, for which the effective mass approximation is valid. The selection rules are found for the intraband level-to-level optical hole transitions. The square of the matrix element of the dipole moment of interlevel hole transitions was calculated, which made it possible to establish that the transitions between states $1S_{3/2}$ and $1P_{3/2}$ are less probable than those between states $1S_{3/2}$ and $1P_{5/2}$.

Squares of matrix elements of the dipole moment of interlevel hole transitions $|\mathbf{D}_{mn}|^2$ (in Å ^{2} units) for various QD radii

	$1S_{3/2} \leftrightarrow 1P_{3/2}$		$1S_{3/2} \leftrightarrow 1P_{5/2}$	
a Å	$(M'_f = -3/2,$ $M_f = -3/2)$ and $(M'_f = 3/2,$ $M_f = 3/2)$	$(M'_f = -1/2,$ $M_f = -1/2)$ and $(M'_f = 1/2,$ $M_f = 1/2)$	$(M'_f = -3/2,$ $M_f = -3/2)$ and $(M'_f = 3/2,$ $M_f = 3/2)$	$(M'_f = -1/2,$ $M_f = -1/2)$ and $(M'_f = 1/2,$ $M_f = 1/2)$
50	12.6704	1.4078	115.6610	173.4910
100	14.4008	1.6890	305.0300	457.5450
150	23.2407	2.5823	502.6240	753.9360

1. Al.L. Efros and A.L. Efros, Fiz. Tekh. Poluprovodn. **16**, 1209 (1982).
2. G.W. Bryant, Phys. Rev. Lett. **59**, 1140 (1987).
3. N.A. Efremov and S.I. Pokutnyi, Fiz. Tverd. Tela **27**, 48 (1985).
4. V.I. Boichuk and R.Yu. Kubay, Fiz. Tverd. Tela **43**, 226 (2001).
5. V.A. Shchukin, N.N. Ledentsov, P.S. Kop'ev, and D. Bimberg, Phys. Rev. Lett. **75**, 2968 (1995).
6. A.D. Andreev and E.P. O'Reilly, Phys. Rev. B **62**, 15851 (2000).
7. N.V. Tkach, A.M. Makhanets, and G.G. Zegrya, Fiz. Tekh. Poluprovodn. **36**, 543 (2002).
8. Jia-Lin Zhu, Phys. Rev. B **39**, 8780 (1989).
9. Jia-Lin Zhu, Phys. Rev. B **41**, 6001 (1990).
10. Jia-Lin Zhu, Phys. Rev. B **50**, 4497 (1994).
11. Chun-Ching Yang, Li-Chi Liu, and Shih-Hsin Chang, Phys. Rev. B **58**, 1954 (1998).
12. M.V. Tkach, V.A. Golovatskyi, and Ya.M. Berezovskyi, Fiz. Khim. Tverd. Tila **4**, 213 (2003).
13. V.I. Boichuk, I.V. Bilynskyi, and R.Ya Leshko, Ukr. J. Phys. **53**, 991 (2008).
14. V.I. Sheka and D.I Sheka, Zh. Èksp. Teor. Fiz. **51**, 1445 (1966).
15. A. Baldereshi and N.O. Lipari, Phys. Rev. B **8**, 2697 (1973).
16. J.M. Luttinger and W. Kohn, Phys. Rev. **97**, 869 (1955).
17. J.M. Luttinger, Phys. Rev. **102**, 1030 (1956).
18. G.B. Grigoryan, E.M. Kazaryan, A.L. Efros, and T.V. Yazeva, Fiz. Tverd. Tela **32**, 1772 (1990).

19. V.I. Boichuk, I.V. Bilynskyi, and I.O. Shakleina, Semicond. Phys. Quant. Electr. Optoelectron. **8**, 26 (2005).
20. E. Menéndez-Proupin and C. Trallero-Giner, Phys. Rev. B **69**, 125336 (2004).
21. E.P. Pokatilov and V.A. Fonoberov, Phys. Rev. B **64**, 245328 (2001).
22. B.L. Gel'mont and M.I. Dyakonov, Fiz. Tekh. Poluprovodn. **5**, 2191 (1971).
23. Jian-Bai Xia and K.W. Cheah, Phys. Rev. B **59**, 10119 (1999).
24. P. Lawaetz, Phys. Rev. B **4**, 3460 (1971).
25. V.I. Boichuk, R.Yu. Kubay, G.M. Godovanets', and I.S. Shevchuk, Zh. Fiz. Dosl. **10**, 220 (2006).

Received 09.06.09.
Translated from Ukrainian by O.I. Voitenko

ДОСЛІДЖЕННЯ АКЦЕПТОРНОЇ ДОМІШКИ У ЦЕНТРІ СФЕРИЧНОЇ НАНОГЕТЕРОСТРУКТУРИ

В.І. Бойчук, І.В. Білинський, Р.Я. Лешко, І.О. Шаклеіна

Р е з ю м е

Для сферичної наногетероструктури GaSb/AlSb, використовуючи сферичний гамільтоніан 4×4, визначено дискретні стани водневоподібної акцепторної домішки для різних розмірів квантової точки. Проведено порівняння визначених енергій з відповідними енергіями, що одержані без урахування складної структури валентної зони. Обчислення проведено як для скінченного, так і для нескінченного потенціалу на межі гетероструктури. Встановлено правила добору для внутрішньозонних міжрівневих оптичних переходів дірки. Визначено середні відстані та ймовірності переходів дірки як функції розмірів квантової точки.